JGR Atmospheres

RESEARCH ARTICLE
10.1029/2019JD030463

Effect of Aerosols on the Ice Cloud Properties Over the Tibetan Plateau

Yuzhi Liu[1], Shan Hua[1], Rui Jia[1,2], and Jianping Huang[1]

[1]Key Laboratory for Semi-Arid Climate Change of the Ministry of Education, College of Atmospheric Sciences, Lanzhou University, Lanzhou, China, [2]Zibo Meteorological Bureau, Zibo, China

Key Points:
- The inconsistent effects of aerosols on ice cloud properties between daytime and nighttime over the Tibetan Plateau are investigated
- A potential relationship may exist between the aerosol index and ice cloud properties
- Aerosols show dominant influence on daytime ICDR and nocturnal IWP and ICOD

Correspondence to:
J. Huang,
hjp@lzu.edu.cn

Citation:
Liu, Y., Hua, S., Jia, R., & Huang, J. (2019). Effect of aerosols on the ice cloud properties over the Tibetan Plateau. *Journal of Geophysical Research: Atmospheres*, *124*, 9594–9608. https://doi.org/10.1029/2019JD030463

Received 13 FEB 2019
Accepted 3 AUG 2019
Accepted article online 7 AUG 2019
Published online 23 AUG 2019

Abstract With the highlight of environmental problems over the Tibetan Plateau (TP), aerosol pollution and the influence of this pollution on cloud properties are becoming a new area of research. Based on the aerosol index and cloud property parameters derived from satellite observations, in this study, the inconsistent effects of aerosols on ice cloud properties between daytime and nighttime over the TP are investigated. The results indicate that ice clouds are mainly distributed over the TP margin area, especially over the north slope, during both daytime and nighttime. The occurrence frequency of ice cloud is higher during the daytime than during the nighttime over the margin areas of the TP. Similarly, aerosols are mainly concentrated over the northern margin of the TP. A potential relationship may exist between the aerosol index and ice cloud properties. When the aerosol index increases from 0.05 to 0.17, the ice cloud droplet radius (ICDR) during the daytime decreases from 32.1 to 27.9 μm, while the ICDR during the nighttime remains almost constant (approximately 25 μm); furthermore, the ice water path (IWP) during the daytime decreases slightly due to the saturation effect, while the nocturnal IWP increases significantly. The changes in ice cloud optical depth (ICOD) during daytime and nighttime show significant and completely opposite trends. The removal of the influence of meteorological factors showed that aerosols have a more dominant influence than meteorological conditions on ice cloud properties (except for the nocturnal ICDR and IWP during the daytime).

1. Introduction

The aerosols suspended in the atmosphere contain liquid and solid matter in the form of particles (IPCC, 2013), although the atmosphere is mostly composed of gases. Despite the small mass or volume fraction of aerosols in the atmosphere, these aerosols can directly or indirectly influence the radiation budget of the Earth-atmosphere system (Bréon et al., 2002; Jiang & Feingold, 2006), further contributing to weather and climate changes (Rosenfeld et al., 2014). The direct effect of aerosols is induced by the scattering of solar radiation and absorption of solar shortwave and longwave radiation (Davidi et al., 2009; Liu et al., 2011, 2013, 2014). Aerosols indirectly influence the radiation budget by affecting cloud microphysical processes, and this influence is one of the most uncertain radiative factors used to predict the Earth's climate systems (IPCC, 2013).

Since Twomey et al. (1974, 1977) reported that aerosols can act as cloud condensation nuclei to alter the mean droplet size and cloud albedo depending on the aerosol absorption and cloud optical thickness (Feingold et al., 2001; Kaufman & Fraser, 1997), much attention has been paid to this interesting topic (Gryspeerdt et al., 2016; Huang, Lin, et al., 2006, Huang, Wang, et al., 2006, 2007; Kaufman et al., 2005; Kaufman & Koren, 2006; Penner et al., 2004; Ramanathan et al., 2001; Rosenfeld et al., 2002). The aerosol indirect radiative effect includes the “first indirect” effect postulated by Twomey (1974, 1977) and the “second indirect” effect (Albrecht, 1989). Additionally, another type of aerosol-cloud interaction, the so-called “semidirect” effect, is usually caused by absorbing aerosols (Cook & Highwood, 2004; Johnson et al., 2004; Kaufman et al., 2002; Menon et al., 2002) and could accelerate the evaporation of cloud droplets and inhibit convection and cloud formation (Hansen et al., 1997; Koren et al., 2008; Penner et al., 2003). Regarding aerosol-cloud interactions, although there are many studies based on observations (Bréon et al., 2002; Costantino & Bréon, 2010; Guo et al., 2017; Myhre et al., 2007; Peng et al., 2016; Wang et al., 2015; Yan et al., 2014) and model simulations (Gettelman et al., 2015; Li et al., 2008; Zelinka et al., 2014), uncertainty still exists.

©2019. American Geophysical Union. All Rights Reserved.

The Tibetan Plateau (TP) is the highest plateau in the world and is an important moisture source that affects the hydrological cycle (Hansen et al., 2000; Wu et al., 2007) through dynamic and thermal forcings (Boos & Kuang, 2010; Hahn & Manabe, 1975; Ye & Gao, 1979). In the summer, the TP is a significant heat source and moisture island in the atmosphere (Xu et al., 2008). Over the TP, abundant ice clouds are produced. Simultaneously, the TP is drastically affected by natural and anthropogenic aerosol sources, which provide a large number of aerosol particles lifted to the atmosphere over the TP (Huang, Lin, et al., 2006, Huang, Wang, et al., 2006, 2007; Jia et al., 2015; Liu et al., 2015). Additionally, sustained warming over the TP associated with global warming has been reported (Duan & Wu, 2006; Duan & Xiao, 2015; Niu et al., 2004; Rangwala et al., 2009, 2013). Thus, under warmer climate conditions over the TP, the aerosol-cloud interaction is an important physical process contributing to the hydrological cycle surrounding the TP. In recent studies, much effort has been focused on the aerosol (Jia et al., 2018; Liu et al., 2015) and cloud properties (Fujinami & Yasunari, 2001; Hua et al., 2018; Li & Fu, 2005; Sato et al., 2007; Taniguchi & Koike, 2008) over the TP; however, there are few studies on the relationship between aerosols and clouds.

In this study, based on satellite products, we statistically investigated the effects of aerosols on the ice cloud properties over the TP in detail in the daytime and nighttime for the 2000–2015 period, as well as the features of ice clouds and aerosols over the plateau.

2. Data Sets

2.1. Clouds and the Earth's Radiant Energy System

The data used in this study include data from Clouds and the Earth's Radiant Energy System (CERES) CldTypHist_Ed4A, which reformats cloud properties from the CERES-SYN1deg-hour/day/month Ed4A products observed by the Moderate Resolution Imaging Spectroradiometer (MODIS) onboard the Terra and Aqua satellites and 1-hourly geostationary (GEO) Ed4A data into the same cloud types as those of the NASA GISS ISCCP-D2 cloud products. In this product, the cloud properties are averaged into three cloud top pressures and three optical depth bins. The nine cloud types are further subdivided into liquid and ice clouds in the daytime and nighttime. Unlike 3-hourly ISCCP-D2 data, the CldTypHist product is based on hourly cloud observations and has the advantage of obtaining diurnal cycle changes (Minnis et al., 2011; Wielicki et al., 1996). According to the quality assessment of the CERES product (https://ceres.larc.nasa.gov/documents/qa_plan3.1.pdf), the terrain features were considered and corrected accordingly during data processing. Although there are some errors over the plateau, this product shows an overall applicability. Improvements to the CERES cloud algorithm in Ed4 compared to Ed3A include a method to determine the low cloud top height by regional mean boundary apparent lapse rates using collocated Cloud–Aerosol Lidar and Infrared Pathfinder Satellite Observations (CALIPSO) and MODIS data (Sun-Mack et al., 2014), a CO_2-slicing method to retrieve high clouds over low-lying clouds (Chang et al., 2010), and a rough ice crystal model (Yang et al., 2008) to improve ice cloud retrieval.

Here the ice cloud area fraction (ICF), ice cloud droplet radius (ICDR), ice cloud optical depth (ICOD), and ice water path (IWP) data derived from the CldTypHist_Ed4A product with a resolution of 1.0° × 1.0° at a monthly time scale for the 2000–2015 period are used to investigate the effects of aerosols on ice cloud properties over the TP. As the CERES data are available from March 2000, the annual mean cloud properties in 2000 are the averages from March to December of that year.

2.2. Multiangle Imaging Spectroradiometer

The Multiangle Imaging Spectroradiometer (MISR), which was launched into Sun-synchronous polar orbit aboard Terra, can simultaneously view the sunlit Earth at the same point using nine widely spaced angles ranging from 70° aftward to 70° forward with spatial sampling resolutions of 275 and 1,100 m on a global basis. The MISR can retrieve aerosol properties even over highly reflective surfaces, such as deserts, which reduces limitations caused by surface-based observations (Christopher & Wang, 2004; Diner, 1999; Martonchik et al., 2004). In addition to the aerosol optical depth (AOD), the combination of multispectral and multiangle data from MISR can provide information about particle size, shape, and single scattering albedo (Kahn et al., 1998, 2001). In particular, optical depth errors in the Level 2 product frequently occur over snow/ice fields due to low spatial contrast and as a consequence of inadequate cloud screening; these errors are mainly observed over Greenland and Antarctica. Based on

the data introduction (https://eosweb.larc.nasa.gov/sites/default/files/project/misr/quality_summaries/L3_Products_20050513.pdf), observations over Greenland and Antarctica are excluded, and the observations over other regions in the Level 3 global aerosol product of MISR are relatively reliable.

The number of counts in space-time bins are included in the Level 3 data files. The MISR Level 3 AOD and Angström exponent (AE) products from the MIL3 MAE data, which are retrieved from multiple orbits at a monthly time scale and a resolution of 0.5° × 0.5°, are used to calculate the aerosol index and evaluate the aerosol data from MERRA-2 in this study. The aerosol index (AIn), which is defined as the product of the AOD and AE, is also used. The AIn allows for a more accurate quantification of aerosol column number concentration than AOD (Nakajima et al., 2001). The AIn is used to indicate small particles (those that act as cloud condensation nuclei) with a high weight.

2.3. CALIPSO

Cloud-Aerosol Lidar with Orthogonal Polarization, which is onboard CALIPSO, launched in April 2006, can provide nearly continuous measurements of the vertical structure and properties of clouds and aerosols and that are near-coincident with observations from MODIS (Winker et al., 2007). The lidar Level 2 vertical feature mask (VFM) product describes the vertical distributions of clouds and aerosols, lidar lighting, and land/water indicators along the CALIPSO orbit. The spatial resolution for the feature classification flags varies as a function of altitude, with the highest spatial resolutions occurring at the lowest altitudes. The products of version 4.10, which was released on 8 November 2016, better classify aerosols and clouds and include substantial improvements to the aerosol subtyping and lidar ratio selection algorithms compared to the products of version 3; thus, version 4.10 products are used with CloudSat observations to identify the aerosol-ice clouds (Kim et al., 2016; Liu et al., 2009).

2.4. CloudSat

As part of the A-Train constellation of satellites, CloudSat provides the first global survey of cloud profiles and cloud physical properties with seasonal and geographical variations from space. CloudSat data provide a rich information source for the evaluation of cloud properties derived from other satellite sensors, notably but not exclusively from other members of the A-Train. CloudSat flies in an on-orbit formation with CALIPSO satellites with a footprint interval of approximately 15 s, providing near-simultaneous observations. CloudSat Standard Data Products are produced as profiles that consist of 125 vertical bins, each approximately 240 m deep. The footprint of a single CloudSat observation profile is approximately 1.3 km across-track by 1.7 km along track, with along-track sampling spaced every 1.1 km. In this study, considering the availability of CALIPSO/CloudSat product archives, the considered time period is from June 2006 to December 2010.

2.5. MERRA-2

MERRA-2 is a long-term atmospheric reanalysis data set beginning in 1980. This data set provides the first satellite-ERA global reanalysis data by assimilating the space-based observations of aerosols and representing their interactions with other physical processes in the climate system. MERRA-2 provides a multidecadal reanalysis in which aerosol and meteorological observations are jointly assimilated within a global data assimilation system (Gelaro et al., 2017). Recently, Simmons et al. (2014) compared multiannual variability and trends in atmospheric temperature derived from ERA-Interim, JRA-55, and MERRA and found good agreement in the upper troposphere and lower stratosphere but less agreement in the middle stratosphere. Randles et al. (2016) presented an overview evaluation of the aerosol fields produced by MERRA-2 data and noted the key features and limitations of aerosol products. All data of MERRA-2 are collected in a regular longitude-by-latitude grid of 0.625° × 0.5° (Gelaro et al., 2017). In this study, the AOD and AE data from hourly aerosol diagnostics product of tavg1_2d_aer_Nx from MERRA-2 are used to analyze the aerosol effect on ice cloud properties, and monthly meteorological parameters of instM_3d_asm_Np product are used to analyze the meteorological influence on the ice cloud properties.

3. Methodology

CERES monthly data from 2000 to 2015 are used to calculate the frequency of ice cloud occurrences. In this calculation, when the cloud area fraction is greater than 0.1%, the sky is considered cloudy. Taking a grid as

an example, the frequency of ice cloud occurrences ($F(x,y)$) in one grid is the number of ice-cloudy sky ($N_{cf>0.1\%(x,y)}$) divided by the total sample number ($N_{total(x,y)}$) during 2000–2015:

$$F(x,y) = \frac{N_{cf>0.1\%(x,y)}}{N_{total(x,y)}} \times 100\% \quad (1)$$

Here based on the CERES monthly data, when there are no default data available, the total sample number ($N_{total(x,y)}$) equals 192 in one grid for the 2000–2015 period. The ice cloud occurrence frequency in each grid over the TP is calculated.

The CALIPSO Level 2 vertical feature mask product is used to determine the cloud phase and distinguish aerosols. The identification of clouds and aerosols is accomplished by checking the cloudy scenarios from the CloudSat 2B-CLDCLASS product to prevent misjudgment of clouds and aerosols due to high aerosol concentrations. Similar to the method of Wang et al. (2010), we define clouds as aerosol-ice clouds if the distance between clouds and aerosols is up to 60 m in the same VFM profile as the CALIPSO product when the clouds are in the ice phase. Thus, the frequency of dusty ice clouds is calculated. In the cloud phase statistics, high-quality data are included, and data with low/no confidence are excluded.

The first indirect effect of aerosols can be quantitatively illustrated using the relationship between two integral variables (ICOD and IWP) and the ICDR.

The ICOD is defined as follows:

$$\mathrm{ICOD} \approx \mathrm{IWP}\left(\frac{b}{\mathrm{ICDR}} + c\right) \quad (2)$$

where the ICDR is the ratio between the third and second moments of the size distribution, $n(r)$, at radius r. Both b and c are parameters relating to the ice crystal shape.

Assuming that IWP is not a constant, the ICOD response to the aerosol increase in the logarithm form can be expressed as follows:

$$\frac{\log ICOD}{\log AIn} \approx \frac{\log IWP}{\log AIn} + \frac{\log\left(\frac{b}{ICDR} + c\right)}{\log AIn} \quad (3)$$

The impact of aerosols on the ICOD is a combination of responses, including ice cloud droplet size and IWP, in addition to aerosols. Based on the above relation and monthly properties of ice clouds from 2000 to 2015, the empirical constants b and c are obtained by numerical fitting. The fitting result shows that over the TP, parameters b and c can be taken as 4.61 and 0.06, respectively. Correspondingly, equation (3) can be approximated as follows:

$$\frac{\log ICOD}{\log AIn} \approx \frac{\log IWP}{\log AIn} + \frac{\log\left(\frac{4.61}{ICDR} + 0.06\right)}{\log AIn} \quad (4)$$

where the units of the ICDR and IWP are μm and g/m^2, respectively. The magnitude of the ICDR is on the order of 10. The value of parameter c is much smaller than the ICDR and can be ignored. Thus, equation (4) can be approximated as follows:

$$\frac{\log ICOD}{\log AIn} \approx \frac{\log(4.61 IWP)}{\log AIn} - \frac{\log(ICDR)}{\log AIn} \quad (5)$$

In the following section, based on equation (5), the effects of aerosols on ice cloud properties are analyzed. Considering the spatial diversity of satellite data, we adopt the bilinear interpolation method to unify all of the satellite data to a common resolution of 1.0° × 1.0°. Then, the logarithmic relationship is investigated for the corresponding grid.

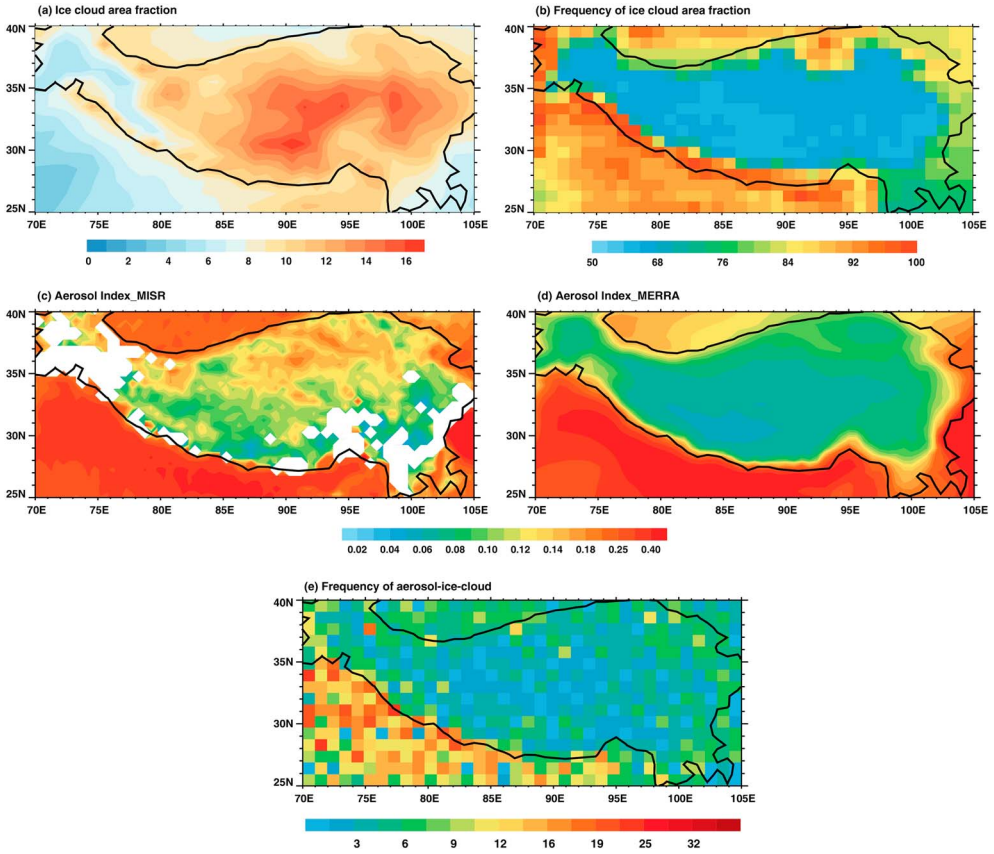

Figure 1. Distribution of the (a) ICF and (b) frequency of the ICF derived from CERES when the ICF is larger than 0.1%, annual mean AIn derived from (c) MISR observations and (d) MERRA data during the 2000–2015 period, and (e) aerosol-ice_cloud data obtained from CALIPSO and CloudSat observations during 2007–2010 over the TP. The area enclosed by the black bold outline indicates the main body of the TP.

4. Results

4.1. Aerosol and Cloud Properties

The TP is located in central East Asia (25–45°N, 70–105°E) and has an average elevation of 4,500 m. In this study, the main body of the TP, which is enclosed by the thick black bold outline in each contour figure, is the region ranging from 25–45°N, 70–105°E, where the elevation exceeds 2,000 m. Zhao et al. (2014) noted that the high-value areas of the IWP are in the central, northern, and western parts of the TP, and ice-phase clouds are dominant over these areas. The satellite observations show that the ICF of the ice clouds is greater than that of the water clouds in both the daytime and nighttime over the TP during 2000–2015 (figures omitted). Therefore, in this study, the analyses mainly focused on the ice clouds over the TP.

Before discussing the ICF frequency distribution, the distribution of the ICF derived from CERES observations is analyzed, as shown in Figure 1a. Overall, high ICFs are concentrated in the central TP, which is in agreement with the results of Zhao et al. (2014). Furthermore, Figure 1b shows the frequency of the annual mean ICF over the TP during the 2000–2015 period. When the ICF is greater than 0.1% in one grid, a cloud is considered to occur in the grid, and then, the statistical frequency is added by individual grid. With decreasing distance to the edge of the plateau, the frequency of ice cloud occurrence increases, even reaching 100% over the southern plateau edge. The distribution of the annual mean AIn derived from MISR observations over the TP during the 2000–2015 period is shown in Figure 1c. As shown in Figure 1c, the AIn increases gradually from south to north over parts of the TP, with a minimum value (0.01) over the southern margin and a maximum value (0.62) over the northern margin. The high values of the AIn are mainly distributed

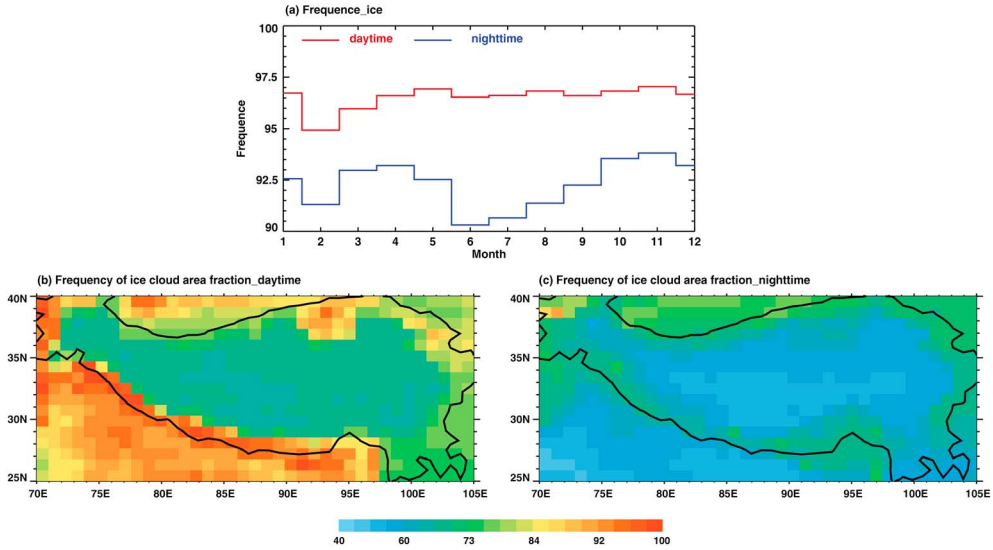

Figure 2. (a) Monthly mean histogram of ICF during 2000–2015. (b) Frequency (%) of annual mean ICF in the daytime over the TP during 2000–2015. (c) Same as (b) but for nighttime. ICF is derived from CERES product. The area enclosed by the black bold outline indicates the main body of the TP.

over the northern slope of the TP, and the index peaks at 0.2. Similar to the MISR observations, in Figure 1d, the distribution of the annual mean AIn derived from MERRA over the TP during the 2000–2015 period is consistent with that shown in Figure 1c. In the following analyses, as MERRA provides aerosol data in the daytime and nighttime separately, we analyze the aerosol properties and the relation between aerosols and ice cloud properties using MERRA data. Combining Figures 1b–1d, we find that both ice clouds and aerosols frequently occur over the margin areas of the plateau, especially over the northern slope of the TP. This finding, that is, that there is a mixture of aerosols and ice clouds over the margin areas of the TP, implies that aerosols affect ice clouds. Figure 1e shows the distribution of the aerosol and ice cloud mixture (hereafter called aerosol-ice_cloud) obtained from CALIPSO and CloudSat observations over the TP during 2007–2010. Here considering the high quality of data covering 2007–2010, the frequency distribution of aerosol-ice_cloud during the period of 2007–2010 is analyzed. The frequency of aerosol-ice_cloud is higher over the margin areas of the plateau than over the central TP. As shown in Figures 1b and 1e, the frequency of the ICF and the aerosol-ice_cloud over the TP agree. Therefore, it is possible that aerosols affect the ice cloud properties due to being mixed.

Figure 2 shows the frequency of ice clouds in the daytime and nighttime over the TP during 2000–2015. The monthly mean ICF during the 2000–2015 period is shown in Figure 2a. The frequencies of ice clouds in the daytime and nighttime are indicated by red and blue lines, respectively. Obviously, the ice cloud occurrence frequency in the daytime is much higher than that in the nighttime. During the daytime, with increasing solar radiation at the surface, the sensible heat and surface temperature increase. Due to this heating, the convergence of ascending motions easily occurs, which drives warm and humid air to lift to higher altitudes. The air temperature decreases with the increases in altitude at a rate of 0.65 K/km. Thus, the higher the warm-humid air is lifted from the surface, the colder the air temperature is and the more ice clouds are formed. In contrast, because the surface becomes cold due to the emission of thermal radiation in the nighttime, these conditions are unfavorable for the formation of ice clouds in the nighttime. Overall, the heating difference between the daytime and nighttime may be the main reason for the large discrepancy in the ICF frequency over the TP. In addition, there is a considerable discrepancy between the monthly variations in the daytime and nighttime. In the daytime, ice clouds occur the least frequently in February (95%), while ice clouds occur the most frequently in November (97%). However, in the nighttime, the ice cloud frequency continually increases from June to November, with the lowest frequency in June (91%) and the highest frequency in November (94%). Figures 2b and 2c show the frequency distributions of the annual mean ICFs in the daytime and nighttime, respectively. According to the distributions, the ice cloud

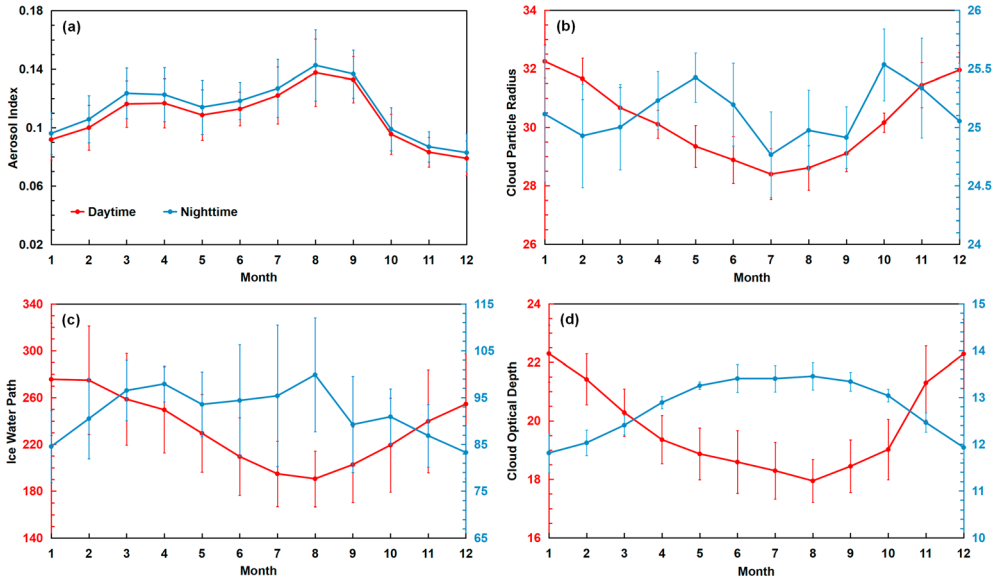

Figure 3. Monthly mean AIn and cloud parameters over the TP during the 2000–2015 period. (a–d) AIn, ICDR, IWP, and ICOD, respectively. AIn is calculated by the data of AOD and AE derived from MERRA-2. ICDR, IWP, and ICOD are derived from CERES product. The red lines represent daytime ice clouds, and the blue lines represent nighttime ice clouds. Error bars represent the standard deviation of monthly mean values.

occurrence frequency in the daytime (Figure 2b) is higher overall than that in the nighttime (Figure 2c). Additionally, during both daytime and nighttime, the lowest ice cloud frequency occurs near the center of the TP. In view of the diurnal difference between ice cloud occurrences, the aerosol effects on ice clouds in the daytime and nighttime over the TP during 2000–2015 are separately investigated in the following analysis.

Figure 3 shows the monthly mean AIn, ICDR, IWP, and ICOD over the TP during the 2000–2015 period. The AIn and ice cloud properties in the daytime and nighttime are indicated by red and blue lines, respectively. As shown in Figure 3a, the AIn increases beginning in January, peaks in March and August, and then decreases over the TP. The AIns in the daytime and nighttime show similar monthly cycles. Overall, high AIns are concentrated in the spring and summer. In Figures 3b–3d, the minimum ICDR, ICOD, and IWP in the daytime occur in July, August, and August, respectively. As the AIn increases, the ICOD, ICDR, and IWP decrease. Additionally, the diurnal and nocturnal variations in ICDR, ICOD, and IWP show great discrepancies. In particular, the monthly variations in ICOD during the daytime and nighttime are opposite.

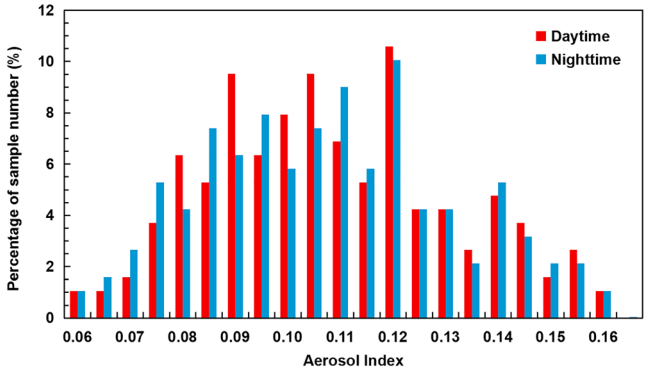

Figure 4. Percentage (%) of samples in different AIn bins out of the total number of samples. The red and blue bars represent the sample number percentages during the daytime and nighttime, respectively. The AIn is calculated by the data of AOD and AE derived from MERRA-2.

4.2. Aerosol Effect on Cloud Microphysical Properties

In view of the influence of uneven sample distribution on the fitted slope between the aerosols and clouds, the sample weight for each AIn bin of all samples is considered. Figure 4 shows the sample percentages for different AIn bins among all samples. The red and blue bars represent percentages in the daytime and nighttime, respectively. Overall, a normal sample percentage distribution, with the AIn values ranging from 0.06 to 0.17, is found during both the daytime and nighttime; the percentage of samples peaks in the AIn bin of 0.12. The aerosols are mainly distributed in AIn bins ranging from 0.075 to 0.145 over the TP. To avoid the influence of the uneven distribution of samples on the fitting slope, in the

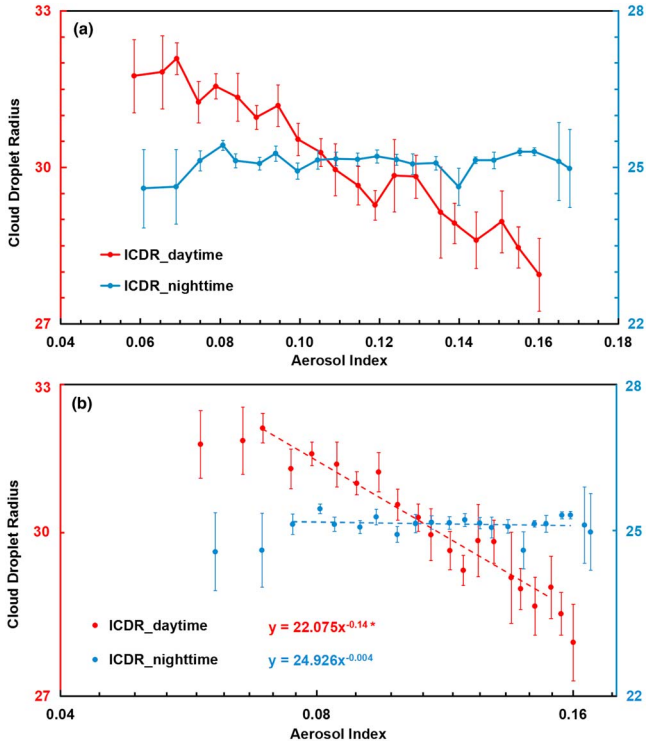

Figure 5. (a) Monthly mean ICDR values for constant bins of the AIn for daytime (red) and nighttime (blue). Error bars represent the confidence levels of the mean values, assuming independent data. Errors are calculated as $s/(n-2)^{1/2}$, where n is the sample number of cloud droplet radius measurements within the bin and s is the standard deviation. (b) Monthly mean ice cloud particle radius values for constant bins of the AIn at the log-log scale. Asterisk indicates that the correlation is significant at the 90% confidence level. The AIn is calculated by the data of AOD and AE derived from MERRA-2, and ICDR is derived from CERES product.

following analyses, we perform the linear fit analysis on bins with a sample weight exceeding 2%.

Figure 5 shows the relation between the ICDR and AIn, with aerosol and cloud samples divided into daytime and nighttime data. The daytime and nocturnal ICDR are shown in red and blue, respectively. As presented in Figure 5a, with increasing AIn, the ICDR decreases for both the daytime and nighttime, which agrees with the "Twomey effect" (the first indirect effect of aerosols). The bins with small sample weights in Figure 4 correspond to high uncertainties in the relation between ICDR and AIn. For ice clouds in the daytime, the ICDR decreases by approximately 14%, from 32.1 to 27.9 μm, as the AIn varies from 0.05 to 0.17. In contrast, the nocturnal ICDR shows stability, with an almost constant value of approximately 25 μm in all of the AIn bins. Figure 5b shows the ICDR averaged over the constant bin of AIn ranging from 0.05 to 0.28 (by a step of 0.01) on the log-log scale. The impact of aerosols on the ICDR can be quantified by the linear regression slope of the ICDR-AIn relationship on a log-log scale. The logarithmic relationships between ICDR and AIn for daytime and nighttime are nearly linear. In the daytime, the ICDR shows a sensitive response to AIn, which is expressed by the best fit slope of −0.14. However, a less sensitive response (−0.004) is found at night. Overall, the effect of aerosols on ICDR in the daytime is more pronounced than that of aerosols on ICDR in the nighttime.

Figure 6 shows the relation between the IWP averaged over the TP and the AIn. As shown in Figure 6a, the daytime IWP decreases slightly (from 255 to 216 g/m^2) as the AIn increases from 0.05 to 0.17, showing little dependence on the AIn. The linear slope between the daytime IWP and AIn on the log-log scale is equal to −0.01 (Figure 6b). Such weak reduction of IWP with increasing AIn is mainly due to the saturation effect, which has been well recognized by previous satellite-based aerosol-cloud interaction studies (Guo et al., 2017; Koren et al., 2014; Wang et al., 2015). Overall, with increasing aerosol particles, the daytime IWP does not increase indefinitely. As shown in Figure 6, the threshold of AIn in above saturation effect over the TP is 0.12. When the AIn increases from 0.05 to 0.12, the daytime IWP indicates increase; however, it decreases as the AIn increases from 0.12 to 0.17. The regression analyses show increase in daytime IWP at a slope of 0.15 under low aerosol loading (AIn < 0.12), but decrease at a slope of −0.06 under high aerosol loading (AIn > 0.12; figure omitted). Such saturation effect could be due to the feedback of intense vapor competitions of aerosol particles under the high aerosol concentration circumstances and the evaporation of small cloud particles associated with more aerosols (Wang et al., 2015). Otherwise, the nocturnal IWP increases significantly (Figure 6a), and the linear slope of the IWP-AIn relationship is equal to 0.29 on the log-log scale (Figure 6b). Compared with the ICDR-AIn relationship, the aerosol effect on the IWP in the nighttime is more pronounced than that in the daytime. As illustrated above, the linear slopes of the daytime ICDR-AIn and IWP-AIn are −0.14 and −0.01, respectively, on the log-log scale. Based on equation (5), the ICOD response to the increase in aerosols can be estimated by the ICDR and IWP. The ICOD-AI relationship may be positive or negative. As shown in Figure 7a, the variations in the daytime and nocturnal ICOD values are completely opposite. The ICOD is strongly dependent on the AIn in the daytime and nighttime. Figure 7b shows that the linear slope of daytime ICOD with AIn is −0.16 on the log-log scale. In the nighttime, the linear slope is equal to 0.13. In addition, Figure 7 indicates that the magnitudes of ICOD variations during the daytime and nighttime are comparable, which suggests that the aerosol effects on ICOD during the daytime and nighttime have a similar order of magnitude. Meanwhile, similar to the daytime IWP (Figure 6), the saturation effect is also found in the daytime ICOD with the change of aerosol. When the AIn increases from 0.05 to 0.12, the daytime ICOD decreases significantly and reaches saturation at AIn = 0.12. The regression analyses show decrease in daytime

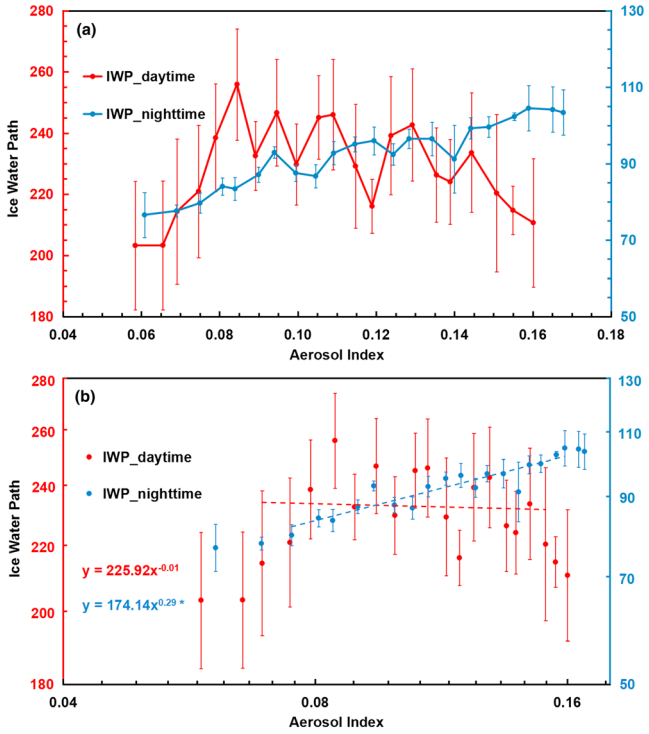

Figure 6. Same as in Figure 5 but for the IWP.

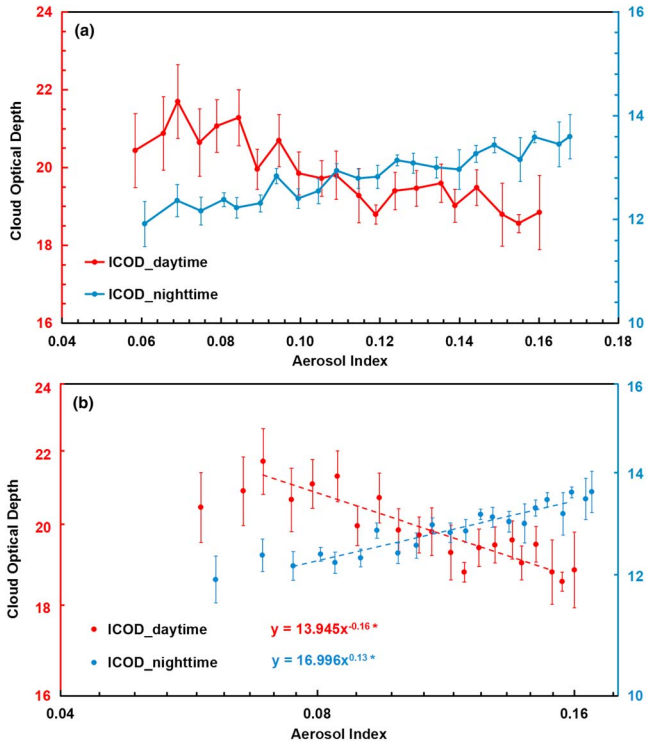

Figure 7. Same as in Figure 5 but for the ICOD.

ICOD at slope of −0.201 under low aerosol condition (AIn < 0.12) but a stable variation at a slope of −0.06 under high aerosol condition (AIn > 0.12; figure omitted).

4.3. Aerosol Effect With the Meteorological Influence Screened Off

In addition to the aerosol effects, the meteorological condition can also cause large-scale cloud changes. For example, cloud properties are usually correlated with the relative humidity and large-scale vertical velocity (Fan et al., 2007). To eliminate the influence of meteorological factors, the partial correlation coefficients between the AIn and ice cloud parameters are calculated. The partial correlation is defined as the correlation between two variables calculated without the influence of other variables. In this way, the influence of other variables can be removed. Here the temperature, pressure, humidity, and wind field are considered. The details of the meteorological factors are listed in Table 1.

Total and partial correlations between the AIn and ice cloud parameters over the TP are shown in Figure 8. When the signs of total and partial correlation coefficients are consistent, the correlations between AIn and cloud parameters are dominant, and the meteorological effect can be neglected. Conversely, if the sign of the partial correlation coefficient is inconsistent with the total correlation, the effect of the meteorological factor is significant. As shown in Figure 8a, the sign of partial correlation between the AIn and daytime ICDR, considering each meteorological factor, is consistent with the total correlation and significant above the 90% confidence level, which suggests that the meteorological condition is not dominant in influencing daytime ICDR. Similar to daytime ICDR, meteorological factors do not have a dominant influence on the relationship between the AIn and nocturnal IWP/ICOD (Figures 8b and 8c). In addition, regarding the correlation between the AIn and nocturnal ICDR, the total correlation and most of the partial correlations are not significant above the 90% confidence level. Furthermore, except for U and w, the aerosol effect on the daytime ICOD is dominant over the effect of meteorological factors. Overall, although the meteorological conditions may affect cloud parameters to some degree, aerosols have a dominant effect on the daytime ICDR, nocturnal IWP, and ICOD. However, the impact of meteorological conditions on the nocturnal ICDR and daytime IWP dominates the aerosol effect. Combined with Figure 8 and Figures 5–7, these results suggest that aerosols dominantly affect ice clouds, except for the nocturnal ICDR and daytime IWP.

Meanwhile, as given in Figure 8a, the daytime ICDR has negative relationships both with AIn and meteorological variables, which confuses the attributions of aerosol and meteorological variables to the changes in ice cloud properties. Further analysis on the total correlation coefficients between AIn and ICDR parameters and partial correlations after screening off the influence of 16 meteorological variables under the low (AIn < 0.12) and high (AIn > 0.12) aerosol loading is performed. As illustrated in Figure 9, under the low aerosol concentration (AIn < 0.12), the aerosol effect on the daytime ICDR indicates more significant than those of meteorological factors. With the increase of aerosol (AIn > 0.12), the U component of wind field partially affects the ICDR, although the partial correlations are not significant at the 90% confidence level. Thus, the daytime ICDR variation is dominantly attributable to the aerosol.

Table 1
Details of the Meteorological Factors in This Study

Abbreviation	Full name	Abbreviation	Full name
U_400	*U* component of winds at 400 hPa	RH_400	Relative humidity at 400 hPa
U_300	*U* component of winds at 300 hPa	RH_300	Relative humidity at 300 hPa
U_200	*U* component of winds at 200 hPa	RH_200	Relative humidity at 200 hPa
V_400	*V* component of winds at 400 hPa	Temp_400	Temperature at 400 hPa
V_300	*V* component of winds at 300 hPa	Temp_300	Temperature at 300 hPa
V_200	*V* component of winds at 200 hPa	Temp_200	Temperature at 200 hPa
w_400	Vertical velocity at 400 hPa	P_sfc	Surface pressure
w_300	Vertical velocity at 300 hPa		
w_200	Vertical velocity at 200 hPa		

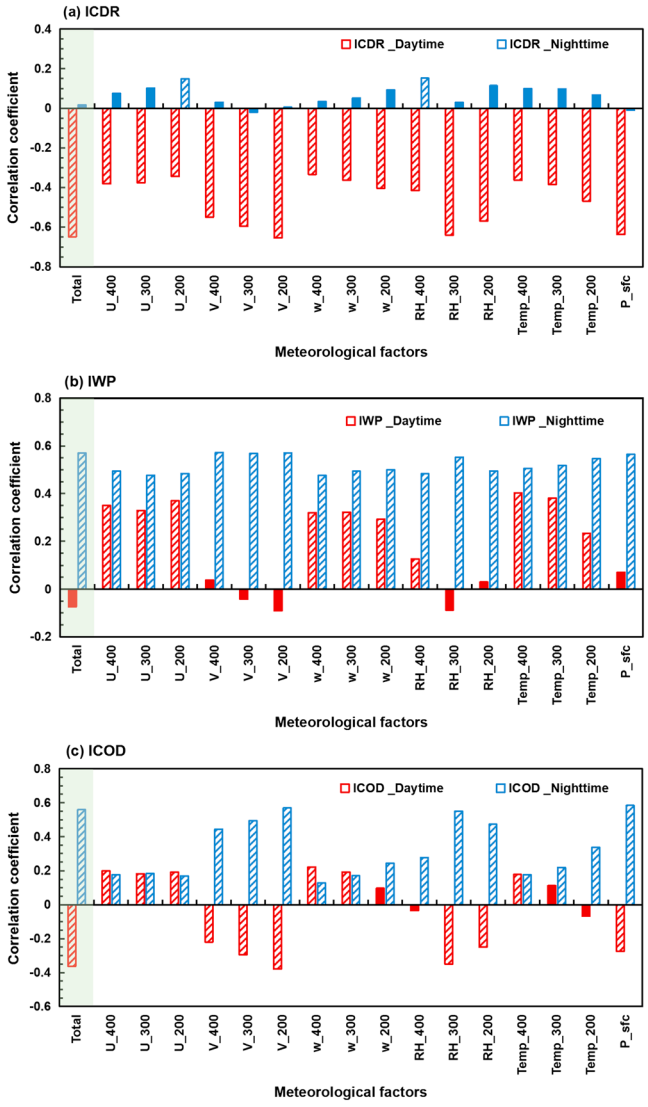

Figure 8. Total correlation coefficients (green shadow) between AIn and ice cloud property parameters and partial correlations after the influence of 16 meteorological factors over the TP had been screened individually. Red and blue represent the correlation coefficients during daytime and nighttime, respectively. The *x* axis indicates the screened meteorological factors. Each bar with oblique lines indicates that the correlation coefficient is significant above the 90% confidence level. The AIn is calculated by the data of AOD and AE derived from MERRA-2, and meteorological factors are also derived from MERRA-2. ICDR and ICOD are derived from CERES product.

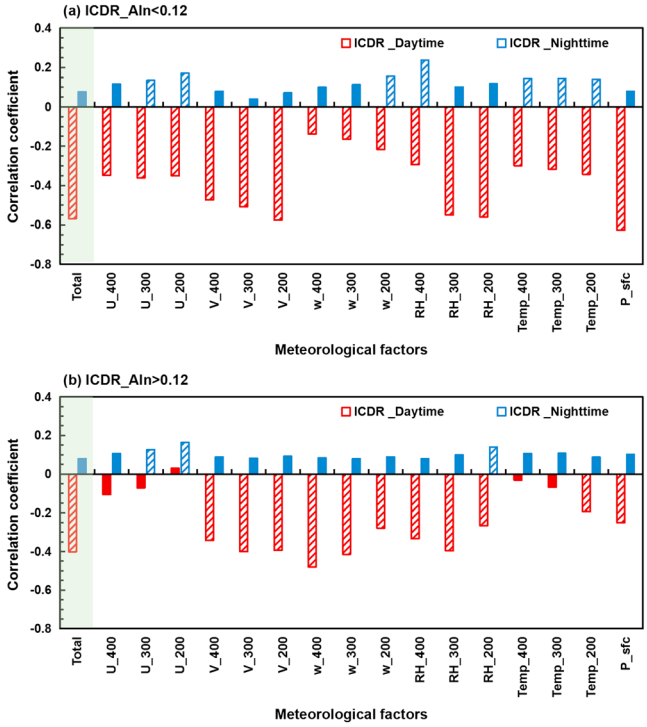

Figure 9. Same as in Figure 8a but for low (AIn < 0.12) and high (AIn > 0.12) aerosol conditions. The bar with oblique lines indicates that the correlation coefficient is significant above the 90% confidence level. The AIn is calculated by the data of AOD and AE derived from MERRA-2, meteorological factors are derived from MERRA-2, and ICDR is derived from CERES product.

5. Conclusion and Discussion

The effects of aerosols on ice cloud properties in the daytime and nighttime over the TP were investigated in this study. We found that ice clouds are mainly distributed over the margin areas of the plateau. The AIn gradually increases from south to north over the TP, with a minimum (0.01) over the southern margin and a maximum (0.62) over the northern margin. Further analysis indicated that aerosol-ice_clouds appear more frequently over the margin area of the plateau than over the central TP.

The cloud property responses to increases in the AIn over the TP were investigated further. The daytime ICDR decreases from 32.1 to 27.9 μm when the AIn increases from 0.05 to 0.17. Otherwise, the nighttime ICDR remains nearly constant, with a value close to 25 μm for all AIn bins. The daytime IWP decreases slightly with increasing AIn, which implies that daytime IWP is not dependent on the AIn. In contrast, the nocturnal IWP increases significantly with increasing AIn. In other words, the aerosol effect on the nocturnal IWP is more pronounced than that on the diurnal IWP. Furthermore, reverse variations in the daytime and nocturnal ICODs with increasing AIn are found. In addition, the ICOD variation magnitudes during the daytime and nighttime, with AIn values ranging from 0.05 to 0.17, are comparable. Especially, the saturation effect could be found in daytime IWP and ICOD. Although the above results provide some evidence about the relationship between aerosol and cloud properties, the effects of meteorological factors on cloud properties cannot be excluded. By calculating the partial correlation coefficient between the AIn and cloud parameters after screening off the influence of meteorological factors individually, it was found that the aerosol factor has a dominant role in influencing the daytime ICDR, nocturnal IWP, and ICOD over the meteorological factors.

In addition to influencing cloud properties, aerosols can affect the radiation budget and impact the vertical motions of the atmosphere and cloud development. As reported by previous studies (Huang et al., 2007; Jia et al., 2015), dust is the dominant aerosol type over the TP because the TP is located at the junction of several dust sources, including the Taklimakan desert, Gurbantunggut desert, and Great Indian Thar desert. The

absorption feature of transported dust may contribute to atmospheric heating and surface cooling (Jia et al., 2018) and significantly accelerate snow melting and the vertical thermal structure over the TP (Lau et al., 2010; Wu et al., 2002, 2006). Due to surface cooling and heating in the atmosphere induced by dust aerosols, the stability of the atmosphere is enhanced, causing an accumulation of dust particles in the atmosphere and influencing the development of clouds. The heating effect due to dust aerosols makes supersaturation and cloud development difficult; additionally, heating may contribute to cloud dissipation by the evaporation process (Fan et al., 2008). Especially, a much more significant effect of dust aerosol on the shortwave radiation than the longwave radiation has been found (Jia et al., 2015), which implies a more obvious heating effect due to the daytime dust aerosol than that of the nighttime. During the daytime, due to the heating effect of dust aerosol, an enhanced evaporation of the cloud particles could be induced, providing dust aerosol with more water vapor in nucleation process. With the increase in dust aerosol, the competition for the water vapor is intensified, resulting in a more significant decrease of daytime ICDR. Consequently, the daytime IWP responds quickly to the increase in dust aerosol, showing a significant increase and a saturation effect as the dust aerosol increases to a threshold (AIn = 0.12). Finally, the changes in ICDR and IWP commonly lead to the change in ICOD and saturation effect. On the contrary, in the nighttime, under a relative stable water vapor environment relating to a less heating effect of dust aerosol, the ICDR remains stable, leading to different changes in IWP and ICOD from the daytime ones. Therefore, aerosols affect cloud features through not only microphysical but also dynamic processes.

Although satellite observations provide valuable information on the relationship between aerosol and ice cloud properties over the TP, some uncertainties related to the observations and retrieval algorithms remain. The retrieval algorithm of GEO/MODIS products may be part of the reason for the discrepancy between daytime and nighttime cloud properties. The daytime cloud properties of MODIS and GEO are retrieved from both visible and infrared bands, while the nocturnal cloud properties are retrieved from infrared bands only. It is very difficult to obtain accurate optical depths for thick clouds using infrared channels only. Moreover, compared with the more reliable daytime retrievals, the nocturnal ICF and IWP are underestimated. The difference between the ice cloud properties from GEO and MODIS may be partially caused by diurnal variations. However, since the current climate model cannot provide sufficient evidence on comprehensive ice core effects with the cloud resolving scheme, satellite observations at present provide a method to understand aerosol effects on ice clouds.

In conclusion, regarding the aerosol effect on ice cloud properties over the TP, although some interesting phenomena were obtained from satellite observations, huge uncertainties remain. It is urgent to reveal the nature of the aerosol-cloud relationship in future studies via a comprehensive investigation combining high-resolution model simulations and reliable observations over the TP.

Acknowledgments
This research was mainly supported by the Strategic Priority Research Program of the Chinese Academy of Sciences (grant XDA2006010301) and the National Natural Science Foundation of China (91737101, 91744311, and 41521004). The authors are grateful to the following science teams for providing the accessible data products used in this study. The CERES and MISR data sets were obtained from the NASA Langley Research Center Atmospheric Science Data Center, https://eosweb.larc.nasa.gov/. The CALIPSO products were obtained from the NASA Langley Research Center Atmospheric Science Data Center (https://www-calipso.larc.nasa.gov/). The CloudSat products were accessible through the CloudSat Data Processing Center website at http://www.cloudsat.cira.colostate.edu/data-products. MERRA-2 data were provided by the Global Modeling and Assimilation Office (GMAO) at the NASA Goddard Space Flight Center through the NASA GES DISC online archive (https://disc.sci.gsfc.nasa.gov/daac-bin/FTPSubset2.pl). All the data used are listed in the references.

References

Albrecht, B. A. (1989). Aerosols, cloud microphysics, and fractional cloudiness. *Science*, *245*(4923), 1227–1230. https://doi.org/10.1126/science.245.4923.1227

Boos, W. R., & Kuang, Z. (2010). Dominant control of the South Asian monsoon by orographic insulation versus plateau heating. *Nature*, *463*(7278), 218–222. https://doi.org/10.1038/nature08707

Bréon, F. M., Tanré, D., & Generoso, S. (2002). Aerosol effect on cloud droplet size monitored from satellite. *Science*, *295*(5556), 834–838. https://doi.org/10.1126/science.1066434

Chang, F. L., Minnis, P., Ayers, J. K., Mcgill, M. J., Palikonda, R., Spangenberg, D. A., et al. (2010). Evaluation of satellite-based upper troposphere cloud top height retrievals in multilayer cloud conditions during TC4. *Journal of Geophysical Research*, *115*, D00J05. https://doi.org/10.1029/2009JD013305

Christopher, S. A., & Wang, J. (2004). Intercomparison between multi-angle imaging spectroradiometer (MISR) and Sun photometer aerosol optical thickness in dust source regions over China: Implications for satellite aerosol retrievals and radiative forcing calculations. *Tellus Series B: Chemical and Physical Meteorology*, *56*(5), 6. https://doi.org/10.1111/j.1600-0889.2004.00120.x

Cook, J., & Highwood, E. J. (2004). Climate response to tropospheric absorbing aerosols in an intermediate general-circulation model. *Quarterly Journal of the Royal Meteorological Society*, *130*(596), 175–191. https://doi.org/10.1256/qj.03.64

Costantino, L., & Bréon, F. (2010). Analysis of aerosol-cloud interaction from space. *Geophysical Research Letters*, *37*, L11801. https://doi.org/10.1029/2009GL041828

Davidi, A., Koren, I., & Remer, L. (2009). Direct measurements of the effect of biomass burning over the amazon on the atmospheric temperature profile. *Atmospheric Chemistry and Physics*, *9*(21), 8211–8221. https://doi.org/10.5194/acp-9-8211-2009

Diner, J. D. (1999). MISR level 2 aerosol retrieval algorithm theoretical basis. Rev. D, JPL-D11400, Jet Propulsion Laboratory, Pasadena, California.

Duan, A., & Wu, G. (2006). Change of cloud amount and the climate warming on the Tibetan Plateau. *Geophysical Research Letters*, *33*, L22704. https://doi.org/10.1029/2006GL027946

Duan, A., & Xiao, Z. (2015). Does the climate warming hiatus exist over the Tibetan Plateau? *Scientific Reports*, *5*(1), 13711. https://doi.org/10.1038/srep13711

Fan, J., Zhang, R., Li, G., & Tao, W. K. (2007). Effects of aerosols and relative humidity on cumulus clouds. *Journal of Geophysical Research*, *112*, D14204. https://doi.org/10.1029/2006JD008136

Fan, J., Zhang, R., Tao, W. K., & Mohr, K. I. (2008). Effects of aerosol optical properties on deep convective clouds and radiative forcing. *Journal of Geophysical Research*, *113*, D08209. https://doi.org/10.1029/2007JD009257

Feingold, G., Remer, L. A., Ramaprasad, J., & Kaufman, Y. J. (2001). Analysis of smoke impact on clouds in Brazilian biomass burning regions: An extension of Twomey's approach. *Journal of Geophysical Research*, *106*(D19), 22907–22922. https://doi.org/10.1029/2001JD000732

Fujinami, H., & Yasunari, T. (2001). The seasonal and intraseasonal variability of diurnal cloud activity over the Tibetan Plateau. *Journal of the Meteorological Society of Japan*, *79*(6), 1207–1227. https://doi.org/10.2151/jmsj.79.1207

Gelaro, R., Mccarty, W., Suárez, M. J., Todling, R., Molod, A., Takacs, L., et al. (2017). The Modern-Era Retrospective Analysis for Research and Applications, version 2 (MERRA-2). *Journal of Climate*, *30*(14), 5419–5454. https://doi.org/10.1175/JCLI-D-16-0758.1

Gettelman, A., Morrison, H., Santos, S., Bogenschutz, P., & Caldwell, P. M. (2015). Advanced two-moment bulk microphysics for global models. Part II: Global model solutions and aerosol–cloud interactions. *Journal of Climate*, *28*(3), 1288–1307. https://doi.org/10.1175/JCLI-D-14-00103.1

Gryspeerdt, E., Quaas, J., & Bellouin, N. (2016). Constraining the aerosol influence on cloud fraction. *Journal of Geophysical Research: Atmospheres*, *121*, 3566–3583. https://doi.org/10.1002/2015JD023744

Guo, J., Su, T., Li, Z., Miao, Y., Li, J., Liu, H., et al. (2017). Declining frequency of summertime local-scale precipitation over eastern China from 1970 to 2010 and its potential link to aerosols. *Journal of Geophysical Research: Atmospheres*, *44*, 5700–5708. https://doi.org/10.1002/2017GL073533

Hahn, D. G., & Manabe, S. (1975). The role of mountains in the South Asian monsoon circulation. *Journal of the Atmospheric Sciences*, *32*(8), 1515–1541. https://doi.org/10.1175/1520-0469(1975)032<1515:TROMIT>2.0.CO;2

Hansen, J., Sato, M., & Ruedy, R. (1997). Radiative forcing and climate response. *Journal of Geophysical Research*, *102*(D6), 6831–6864. https://doi.org/10.1029/96JD03436

Hansen, J., Sato, M., Ruedy, R., Lacis, A., & Oinas, V. (2000). Global warming in the twenty-first century: An alternative scenario. *Proceedings of the National Academy of Sciences*, *97*(18), 9875–9880. https://doi.org/10.1073/pnas.170278997

Hua, S., Liu, Y., Jia, R., Chang, S., Wu, C., Zhu, Q., et al. (2018). Role of clouds in accelerating cold-season warming during 2000–2015 over the Tibetan Plateau. *International Journal of Climatology*, *38*(13), 4950–4966. https://doi.org/10.1002/joc.5709

Huang, J., Lin, B., Minnis, P., Wang, T., Wang, X., Hu, Y., et al. (2006). Satellite-based assessment of possible dust aerosols semi-direct effect on cloud water path over East Asia. *Geophysical Research Letters*, *33*, L19802. https://doi.org/10.1029/2006GL026561

Huang, J., Minnis, P., Yi, Y., Tang, Q., Wang, X., Hu, Y., et al. (2007). Summer dust aerosols detected from CALIPSO over the Tibetan Plateau. *Geophysical Research Letters*, *34*, L18805. https://doi.org/10.1029/2007GL029938

Huang, J., Wang, Y., Wang, T., & Yi, Y. (2006). Dusty cloud radiative forcing derived from satellite data for middle latitude regions of East Asia. *Progress in Natural Science*, *115*(10), 1084–1089. https://doi.org/10.1029/2010JD014109

IPCC (2013). *Climate Change 2013: The Physical Science Basis. Contribution of Working Group I to the Fifth Assessment Report of the intergovernmental panel on climate change*. Cambridge, U. K.: Cambridge University Press.

Jia, R., Liu, Y., Chen, B., Zhang, Z., & Huang, J. (2015). Source and transportation of summer dust over the Tibetan Plateau. *Atmospheric Environment*, *123*, 210–219. https://doi.org/10.1016/j.atmosenv.2015.10.038

Jia, R., Liu, Y., Hua, S., Zhu, Q., & Shao, T. (2018). Estimation of the aerosol radiative effect over the Tibetan Plateau based on the latest CALIPSO product. *Journal of Meteorological Research*, *32*(5), 707–722. https://doi.org/10.1007/s13351-018-8060-3

Jiang, H., & Feingold, G. (2006). Effect of aerosol on warm convective clouds: Aerosol-cloud-surface flux feedbacks in a new coupled large eddy model. *Journal of Geophysical Research*, *111*, D01202. https://doi.org/10.1029/2005JD006138

Johnson, B. T., Shine, K. P., & Forster, P. M. (2004). The semi-direct aerosol effect: Impact of absorbing aerosols on marine stratocumulus. *Quarterly Journal of the Royal Meteorological Society*, *130*(599), 1407–1422. https://doi.org/10.1256/qj.03.61

Kahn, R., Banerjee, P., & Mcdonald, D. (2001). Sensitivity of multiangle imaging to natural mixtures of aerosols over ocean. *Journal of Geophysical Research*, *106*(D16), 18219–18238. https://doi.org/10.1029/2000JD900497

Kahn, R., Banerjee, P., Mcdonald, D., & Diner, D. J. (1998). Sensitivity of multiangle imaging to aerosol optical depth and to pure-particle size distribution and composition over ocean. *Journal of Geophysical Research*, *103*(D24), 32195–32213. https://doi.org/10.1029/98JD01752

Kaufman, Y. J., & Fraser, R. S. (1997). The effect of smoke particles on clouds and climate forcing. *Science*, *277*(5332), 1636–1639. https://doi.org/10.1126/science.277.5332.1636

Kaufman, Y. J., & Koren, I. (2006). Smoke and pollution aerosol effect on cloud cover. *Science*, *313*(5787), 655–658. https://doi.org/10.1126/science.1126232

Kaufman, Y. J., Koren, I., Remer, L. A., Rosenfeld, D., & Rudich, Y. (2005). The effect of smoke, dust, and pollution aerosol on shallow cloud development over the Atlantic Ocean. *Proceedings of the National Academy of Sciences*, *102*(32), 11207–11212. https://doi.org/10.1073/pnas.0505191102

Kaufman, Y. J., Tanré, D., & Boucher, O. (2002). A satellite view of aerosols in the climate system. *Nature*, *419*(6903), 215–223. https://doi.org/10.1038/nature01091

Kim, M. H., Omar, A. H., Vaughan, M. A., Winker, D. M., & Kim, S. W. (2016). Quantifying the low bias of CALIPSO's column aerosol optical depth due to undetected aerosol layers: Undetected aerosols in CALIPSO AOD. *Journal of Geophysical Research: Atmospheres*, *122*, 1098–1113. https://doi.org/10.1002/2016JD025797

Koren, I., Dagan, G., & Altaratz, O. (2014). From aerosol-limited to invigoration of warm convective clouds. *Science*, *344*(6188), 1143–1146. https://doi.org/10.1126/science.1252595

Koren, I., Martins, J. V., Remer, L. A., & Afargan, H. (2008). Smoke invigoration versus inhibition of clouds over the amazon. *Science*, *321*(5891), 946–949. https://doi.org/10.1126/science.1159185

Lau, W. K. M., Kim, M. K., Kim, K. M., & Lee, W. S. (2010). Enhanced surface warming and accelerated snow melt in the Himalayas and Tibetan Plateau induced by absorbing aerosols. *Environmental Research Letters*, *5*(2), 025204. https://doi.org/10.1088/1748-9326/5/2/025204

Li, G., Wang, Y., & Zhang, R. (2008). Implementation of a two-moment bulk microphysics scheme to the WRF model to investigate aerosol-cloud interaction. *Journal of Geophysical Research*, *113*, D15211. https://doi.org/10.1029/2007JD009361

Li, R., & Fu, Y. F. (2005). Tropical precipitation estimated by GPCP and TRMM PR observations. *Advances in Atmospheric Sciences*, *22*(6), 852–864. https://doi.org/10.1007/bf02918685

Liu, Y., Huang, J., Shi, G., Takamura, T., Khatri, P., Bi, J., et al. (2011). Aerosol optical properties determined from sky-radiometer over loess plateau of northwest China. *Atmospheric Chemistry and Physics*, *11*(22), 11455–11463. https://doi.org/10.5194/acp-11-11455-2011

Liu, Y., Jia, R., Dai, T., Xie, Y., & Shi, G. (2014). A review of aerosol optical properties and radiative effects. *Journal of Meteorological Research*, *28*(6), 1003–1028. https://doi.org/10.1007/s13351-014-4045-z

Liu, Y., Sato, Y., Jia, R., Xie, Y., Huang, J., & Nakajima, T. (2015). Modeling study on the transport of summer dust and anthropogenic aerosols over the Tibetan Plateau. *Atmospheric Chemistry and Physics*, *15*(21), 12581–12594. https://doi.org/10.5194/acp-15-12581-2015

Liu, Y., Shi, G., & Xie, Y. (2013). Impact of smoke aerosol on glacial-interglacial climate. *Advances in Atmospheric Sciences*, *30*(6), 1725–1731. https://doi.org/10.1007/s00376-013-2289-7

Liu, Z., Vaughan, M., Winker, D., Kittaka, C., Getzewich, B., Kuehn, R., et al. (2009). The CALIPSO lidar cloud and aerosol discrimination: Version 2 algorithm and initial assessment of performance. *Journal of Atmospheric and Oceanic Technology*, *26*(7), 1198–1213. https://doi.org/10.1175/2009JTECHA1229.1

Martonchik, J. V., Diner, D. J., Kahn, R. A., Gaitley, B. J., & Holben, B. N. (2004). Comparison of MISR and AERONET aerosol optical depths over desert sites. *Geophysical Research Letters*, *31*, L16102. https://doi.org/10.1029/2004GL019807

Menon, S., Hansen, J., Nazarenko, L., & Luo, Y. (2002). Climate effects of black carbon aerosols in China and India. *Science*, *297*(5590), 2250–2253. https://doi.org/10.1126/science.1075159

Minnis, P., Sun-Mack, S., Young, D. F., Heck, P. W., Garber, D. P., Chen, Y., et al. (2011). CERES Edition-2 cloud property retrievals using TRMM VIRS and Terra and Aqua MODIS data, Part I: Algorithms. *IEEE Transactions on Geoscience and Remote Sensing*, *49*(11), 4374–4400. https://doi.org/10.1109/TGRS.2011.2144601

Myhre, G., Stordal, F., Johnsrud, M., Kaufman, Y. J., Rosenfeld, D., Storelvmo, T., et al. (2007). Aerosol-cloud interaction inferred from MODIS satellite data and global aerosol models. *Atmospheric Chemistry and Physics*, *7*(12), 3081–3101. https://doi.org/10.5194/acp-7-3081-2007

Nakajima, T., Higurashi, A., Kawamoto, K., & Penner, J. E. (2001). A possible correlation between satellite-derived cloud and aerosol microphysical parameters. *Geophysical Research Letters*, *28*(7), 1171–1174. https://doi.org/10.1029/2000GL012186

Niu, T., Chen, L., & Zhou, Z. (2004). The characteristics of climate change over the Tibetan Plateau in the last 40 years and the detection of climatic jumps. *Advances in Atmospheric Sciences*, *21*(2), 193–203. https://doi.org/10.1007/BF02915705

Peng, J., Li, Z., Zhang, H., Liu, J., & Cribb, M. C. (2016). Systematic changes in cloud radiative forcing with aerosol loading for deep clouds from multi-year global A-Train satellite datasets. *Journal of the Atmospheric Sciences*, *73*(1), 231–249. https://doi.org/10.1175/JAS-D-15-0080.1

Penner, J. E., Dong, X., & Chen, Y. (2004). Observational evidence of a change in radiative forcing due to the indirect aerosol effect. *Nature*, *427*(6971), 231–234. https://doi.org/10.1038/nature02234

Penner, J. E., Zhang, S. Y., & Chuang, C. C. (2003). Soot and smoke aerosol may not warm climate. *Journal of Geophysical Research*, *108*(D21), 4657. https://doi.org/10.1029/2003JD003409

Ramanathan, V., Crutzen, P. J., Kiehl, J. T., & Rosenfeld, D. (2001). Aerosols, climate, and the hydrological cycle. *Science*, *294*(5549), 2119–2124. https://doi.org/10.1126/science.1064034

Randles, C. A., da Silva, A. M., Buchard, V., Darmenov, A., Colarco, P. R., Aquila, V., et al. (2016). The MERRA-2 aerosol assimilation. Technical Report Series on Global Modeling and Data Assimilation, 45, 1–140.

Rangwala, I., Miller, J. R., & Xu, M. (2009). Warming in the Tibetan Plateau: Possible influences of the changes in surface water vapor. *Geophysical Research Letters*, *36*, L06703. https://doi.org/10.1029/2009GL037245

Rangwala, I., Sinsky, E., & Miller, J. R. (2013). Amplified warming projections for high altitude regions of the northern hemisphere mid-latitudes from CMIP5 models. *Environmental Research Letters*, *8*(2), 024040. https://doi.org/10.1088/1748-9326/8/2/024040

Rosenfeld, D., Lahav, R., Khain, A., & Pinsky, M. (2002). The role of sea spray in cleansing air pollution over ocean via cloud processes. *Science*, *297*(5587), 1667–1670. https://doi.org/10.1126/science.1073869

Rosenfeld, D., Sherwood, S., Wood, R., & Donner, L. (2014). Climate effects of aerosol-cloud interactions. *Science*, *343*(6169), 379–380. https://doi.org/10.1126/science.1247490

Sato, T., Miura, H., & Satoh, M. (2007). Spring diurnal cycle of clouds over Tibetan Plateau: Global cloud-resolving simulations and satellite observations. *Geophysical Research Letters*, *34*, L18816. https://doi.org/10.1029/2007GL030782

Simmons, A. J., Poli, P., Dee, D. P., Berrisford, P., & Peubey, C. (2014). Estimating low-frequency variability and trends in atmospheric temperature using ERA-Interim. *Quarterly Journal of the Royal Meteorological Society*, *140*(679), 329–353. https://doi.org/10.1002/qj.2317

Sun-Mack, S., Minnis, P., Chen, Y., Kato, S., Yi, Y., Gibson, S. C., et al. (2014). Regional apparent boundary layer lapse rates determined from CALIPSO and MODIS data for cloud-height determination. *Journal of Applied Meteorology and Climatology*, *53*(4), 990–1011. https://doi.org/10.1175/JAMC-D-13-081

Taniguchi, K., & Koike, T. (2008). Seasonal variation of cloud activity and atmospheric profiles over the eastern part of the Tibetan Plateau. *Journal of Geophysical Research*, *113*, D10104. https://doi.org/10.1029/2007JD009321

Twomey, S. (1974). Pollution and the planetary albedo. *Atmospheric Environment*, *8*(12), 1251–1256. https://doi.org/10.1016/0004-6981(74)90004-3

Twomey, S. (1977). The influence of pollution on the shortwave albedo of clouds. *Journal of the Atmospheric Sciences*, *34*(7), 1149–1152. https://doi.org/10.1175/1520-0469(1977)034<1149:TIOPOT>2.0.CO;2

Wang, F., Guo, J., Zhang, J., Huang, J., Min, M., Chen, T., et al. (2015). Multi-sensor quantification of aerosol-induced variability in warm cloud properties over eastern China. *Atmospheric Environment*, *113*, 1–9. https://doi.org/10.1016/j.atmosenv.2015.04.063

Wang, W., Huang, J., Minnis, P., Hu, Y., Li, J., Huang, Z., et al. (2010). Dusty cloud properties and radiative forcing over dust source and downwind regions derived from A-Train data during the Pacific dust experiment. *Journal of Geophysical Research*, *115*, D00H35. https://doi.org/10.1029/2010JD014109

Wielicki, B. A., Barkstrom, B. R., Harrison, E. F., Lee, R. B., Smith, G. L., & Cooper, J. E. (1996). Clouds and the Earth's Radiant Energy System (CERES): An Earth Observing System Experiment. *Bulletin of the American Meteorological Society*, *77*(5), 853–868. https://doi.org/10.1175/1520-0477(1996)077<0853:CATERE>2.0.CO;2

Winker, D. M., Hunt, W. H., & Mcgill, M. J. (2007). Initial performance assessment of CALIOP. *Geophysical Research Letters*, *34*, L19803. https://doi.org/10.1029/2007GL030135

Wu, G., Liu, X., Zhang, Q., Mao, J., Liu, Y., & Li, W. (2002). Progresses in the study of the climate impacts of the elevated heating over the Tibetan Plateau. *Climatic and Environmental Research*, *7*(2), 184–201.

Wu, G., Liu, Y., Zhang, Q., Duan, A., Wang, T., Wan, R., et al. (2007). The influence of mechanical and thermal forcing by the Tibetan Plateau on Asian climate. *Journal of Hydrometeorology*, *8*(4), 770–789. https://doi.org/10.1175/jhm609

Wu, G., Mao, J., Duan, A., & Zhang, Q. (2006). Current progresses in study of impacts of the Tibetan Plateau on Asian summer climate. *Journal of Meteorological Research*, *20*(2), 144–158. http://www.cmsjournal.net:8080/Jweb_jmr/EN/

Xu, X., Lu, C., Shi, X., & Gao, S. (2008). World water tower: An atmospheric perspective. *Geophysical Research Letters*, *35*, L20815. https://doi.org/10.1029/2008GL035867

Yan, H., Li, Z., Huang, J., Cribb, M. C., & Liu, J. (2014). Long-term aerosol-mediated changes in cloud radiative forcing of deep clouds at the top and bottom of the atmosphere over the Southern Great Plains. *Atmospheric Chemistry and Physics*, *14*(14), 7113–7124. https://doi.org/10.5194/acp-14-7113-2014

Yang, P., Hong, G., Kattawar, G. W., Minnis, P., & Hu, Y. (2008). Uncertainties associated with the surface texture of ice particles in satellite-based retrieval of cirrus clouds: Part II—Effect of particle surface roughness on retrieved cloud optical thickness and effective particle size. *IEEE Transactions on Geoscience and Remote Sensing*, *46*(7), 1948–1957. https://doi.org/10.1109/tgrs.2008.916472

Ye, D., & Gao, Y. (1979). *The meteorology of the Qinghai-Xizang (Tibet) Plateau*. Beijing: Science Press.

Zelinka, M. D., Andrews, T., Forster, P. M., & Taylor, K. E. (2014). Quantifying components of aerosol-cloud-radiation interactions in climate models. *Journal of Geophysical Research: Atmospheres*, *119*, 7599–7615. https://doi.org/10.1002/2014JD021710

Zhao, Y., Wang, D., & Yin, J. (2014). A study on cloud physical characteristics over the Tibetan Plateau using CloudSat data. *Journal of Tropical Meteorology*, *30*(2), 239–248.